6-7-2018

Localized Deformation in Ni-Mn-Ga Single Crystals

Paul H. Davis
Boise State University

Corey M. Efaw
Boise State University

Lance K. Patten
Boise State University

Courtney Hollar
Boise State University

Chad S. Watson
Boise State University

See next page for additional authors

Localized deformation in Ni-Mn-Ga single crystals

Paul H. Davis,[1] Corey M. Efaw,[1] Lance K. Patten,[1] Courtney Hollar,[2] Chad S. Watson,[1] William B. Knowlton,[1,3] and Peter Müllner[1,a)]

[1]*Micron School of Materials Science and Engineering, Boise State University, Boise, Idaho 83725-2090, USA*
[2]*Department of Mechanical and Biomedical Engineering, Boise State University, Boise, Idaho 83725-2090, USA*
[3]*Department of Electrical and Computer Engineering, Boise State University, Boise, Idaho 83725-2090, USA*

(Received 21 February 2018; accepted 2 May 2018; published online 31 May 2018)

The magnetomechanical behavior of ferromagnetic shape memory alloys such as Ni-Mn-Ga, and hence the relationship between structure and nanoscale magnetomechanical properties, is of interest for their potential applications in actuators. Furthermore, due to its crystal structure, the behavior of Ni-Mn-Ga is anisotropic. Accordingly, nanoindentation and magnetic force microscopy were used to probe the nanoscale mechanical and magnetic properties of electropolished single crystalline 10M martensitic Ni-Mn-Ga as a function of the crystallographic *c*-axis (easy magnetization) direction relative to the indentation surface (i.e., *c*-axis in-plane versus out-of-plane). Load-displacement curves from 5–10 mN indentations on in-plane regions exhibited pop-in during loading, whereas this phenomenon was absent in out-of-plane regions. Additionally, the reduced elastic modulus measured for the *c*-axis out-of-plane orientation was ~50% greater than for in-plane. Although heating above the transition temperature to the austenitic phase followed by cooling to the room temperature martensitic phase led to partial recovery of the indentation deformation, the magnitude and direction of recovery depended on the original relative orientation of the crystallographic *c*-axis: positive recovery for the in-plane orientation versus negative recovery (i.e., increased indent depth) for out-of-plane. Moreover, the *c*-axis orientation for out-of-plane regions switched to in-plane upon thermal cycling, whereas the number of twins in the in-plane regions increased. We hypothesize that dislocation plasticity contributes to the permanent deformation, while pseudoelastic twinning causes pop-in during loading and large recovery during unloading in the *c*-axis in-plane case. Minimization of indent strain energy accounts for the observed changes in twin orientation and number following thermal cycling. *Published by AIP Publishing.* https://doi.org/10.1063/1.5026572

I. INTRODUCTION

Magnetic shape memory alloys (MSMAs), also referred to as ferromagnetic shape memory alloys (FSMAs), have attracted significant scientific and technological interest over the last two decades. In particular, Heusler alloys based on nickel-manganese-gallium (Ni-Mn-Ga) have garnered considerable attention since their large magnetic field induced strain was first reported in 1996.[1] Exhibiting magnetic field induced strains of up to 12%,[2] Ni-Mn-Ga is a promising material for use as the active element in actuating devices.[3–8] Ni-Mn-Ga's shape change is accommodated by growth, through twin boundary motion, of martensite variants preferentially aligned with the applied magnetic field. The twinning stress necessary to initiate magnetic field induced twin boundary movement in Ni-Mn-Ga has been shown to be as low as 0.05 MPa.[9] However, in the presence of sufficient transverse mechanical stress, which—in the absence of a rotating magnetic field—is necessary not only for strain recovery but also for actuator-based applications, magnetic field induced strain is prevented. This transverse mechanical stress threshold, known as the blocking stress, is on the order of ~2–6 MPa.[10–12] While reducing the sample size increases blocking stress up to 10 MPa,[13] fewer twinning dislocations—which are the vehicles that transport preferentially aligned martensite variants—are present at small length scales. As a result, higher stresses may be required to initiate twin boundary movement in smaller samples, competing with the fundamental actuating functionality of Ni-Mn-Ga.[14]

Nanoindentation, either alone or in combination with scanning probe microscopy techniques such as atomic force microscopy (AFM) or magnetic force microscopy (MFM), has previously been applied to Ni-Mn-Ga to (i) evaluate the role of twinning during nanoscale deformations,[15,16] (ii) probe the local elastic properties of twin boundaries,[17] (iii) manipulate the local stray magnetic field for memory applications,[18] (iv) facilitate martensitic transformation for magnetocaloric applications,[19] and (v) demonstrate lattice softening in pre-martensitic Ni-Mn-Ga.[20] Of particular relevance to the current work, Ganor and Shilo showed that nanoindentation techniques can be used to resolve differences in reduced elastic modulus of martensitic Ni-Mn-Ga across 90° twin boundaries.[21] In that work, the authors identified anisotropy in the reduced elastic modulus of Ni-Mn-Ga, where the modulus measured perpendicular to the *c*-axis (i.e., for martensite variants exhibiting an in-plane *c*-axis orientation) was significantly less than that measured parallel to

a)Author to whom correspondence should be addressed: petermullner@boisestate.edu

the *c*-axis (out-of-plane orientation), revealing closure twin variants. Aaltio *et al.*[22] found that "pop-in," an instantaneous increase in displacement with no increase in applied load, occurred during nanoindentation of electropolished Ni-Mn-Ga with an in-plane crystallographic *c*-axis orientation. In contrast, samples that were mechanically polished did not show pop-in behavior. Because the electropolished samples had fewer dislocations available to initiate plastic deformation, the authors hypothesized that the observed pop-in phenomenon was associated with a threshold stress being reached, resulting in dislocation nucleation. While these studies deepened understanding of Ni-Mn-Ga at small length scales, knowledge of the underlying physical mechanisms of nanoscale deformation and the corresponding magnetic response is needed to engineer high work output actuating devices.

To provide additional insight into the complex relationship(s) among mechanical deformation, twinning, and magnetic response over small length scales, in this work, the nanomechanical behavior of two different martensite variants of single crystalline Ni-Mn-Ga samples was evaluated using nanoindentation in concert with the non-destructive techniques of AFM and MFM. AFM and MFM are a powerful combination, as together they can reveal changes in the twin structure and magnetic axis orientation at the nanoscale in response to applied thermomechanical stresses.[15,16,18,23] MFM is particularly useful and instructive in the case of FSMAs such as Ni-Mn-Ga, as it provides the ability to readily identify twins and the orientation of the easy magnetization axis (*c*-axis) at the nanoscale, which is not possible in the case of non-ferromagnetic shape memory alloys such as NiTi (nitinol).

Accordingly, in the current study, instrumented indentation was performed on both crystallographic *c*-axis in-plane and out-of-plane orientations of electropolished Ni-Mn-Ga. To elucidate the impact of twins and twin formation during nanoindentation on deformation behavior and subsequent to recovery, AFM and MFM were used to image the indents at room temperature in the martensite phase both before and after heating the sample through the martensite-austenite phase transition. In addition to Ni-Mn-Ga, the combination of instrumented nanoindentation with a Berkovich diamond tip indenter followed by AFM imaging of the resultant indents has also been used previously in studies on NiTi shape memory alloys to examine indentation recovery on the nanoscale following thermal cycling through the martensite to austenite phase transition.[24–26] However, in contrast to these studies, which identified significant recovery (>30%) following thermal cycling, we observed limited indentation deformation recovery for Ni-Mn-Ga, with even *negative* recovery (i.e., increased indent depth) when nanoindentation was performed on surfaces with a *c*-axis out-of-plane orientation. The combination of nanoindentation, AFM, and MFM, along with thermal cycling, has enabled observations here of significant differences in loading behavior, elastic modulus, and indent recovery following nanoindentation for the two crystallographic orientations, perhaps due to elastic anisotropy and pseudoelastic twinning in the case of the *c*-axis in-plane orientation.

II. EXPERIMENTAL METHODS

A. Sample preparation

Indentations and subsequent AFM and MFM imaging were performed under ambient conditions on a parallelepiped $Ni_{51}Mn_{27}Ga_{22}$ single crystal (AdaptaMat Ltd.) with a 10M martensite structure. The faces of the electropolished sample were parallel to the crystallographic planes with the magnetic *c*-axis direction preferentially aligned in-plane (i.e., parallel to the electropolished surface and perpendicular to the indentation axis) or out-of-plane (i.e., perpendicular to the electropolished surface and parallel to the indentation axis) using a magnetic field of 1–2 T. Further details regarding sample preparation (polishing and magnetic alignment procedures) are given in the supplementary material, including Table S1.

B. Nanoindentation and scanning probe microscopy

A nanomechanical test system (Hysitron TS-75 TriboScope) coupled to a scanning probe microscope (Bruker Dimension 3100) was used to perform indents and measure the sample's nanomechanical properties. Load controlled indentation experiments were conducted using a Berkovich diamond indenter with a 100 nm nominal radius of curvature. As described in greater detail in the supplementary material and shown there in Fig. S1, sets of 5 indents were created in a centered square array pattern using a peak load of either 5 mN or 10 mN (30 s hold time with 10 s linear loading and unloading ramp). The resultant load-displacement curves were fit following the method of Oliver and Pharr[27] to extract the reduced elastic modulus of the sample as described in greater detail in the supplementary material.

Following indentation, high-resolution topography and magnetic phase images of the indentation arrays were obtained using a second scanning probe microscope (Bruker Dimension Icon) operated in the MFM mode. After imaging at room temperature, the Ni-Mn-Ga sample was heated through its martensite-austenite phase transition temperature (70 °C) using a thermoelectric heater-cooler unit (Bruker Nano Thermal Applications Controller) following the approach described in previous work.[23] The sample was held in the austenite phase for 10 min at 81 °C and then cooled to room temperature and reimaged in the MFM mode.

III. RESULTS

A. Nanoindentation

Figure 1 presents representative load-displacement curves for $Ni_{51}Mn_{27}Ga_{22}$ samples with the *c*-axis oriented in-plane versus out-of-plane subjected to maximum loads of 5 mN [Fig. 1(a)] and 10 mN [Fig. 1(b)]. Within statistical uncertainty (i.e., one standard deviation based on 5 measurements per sample), the average reduced elastic modulus (E_r) was independent of indentation load but was approximately 50% greater for the out-of-plane versus in-plane orientation (Table I). The *c*-axis orientation also influenced load-displacement behavior during loading and unloading. Pop-ins [horizontal load-displacement

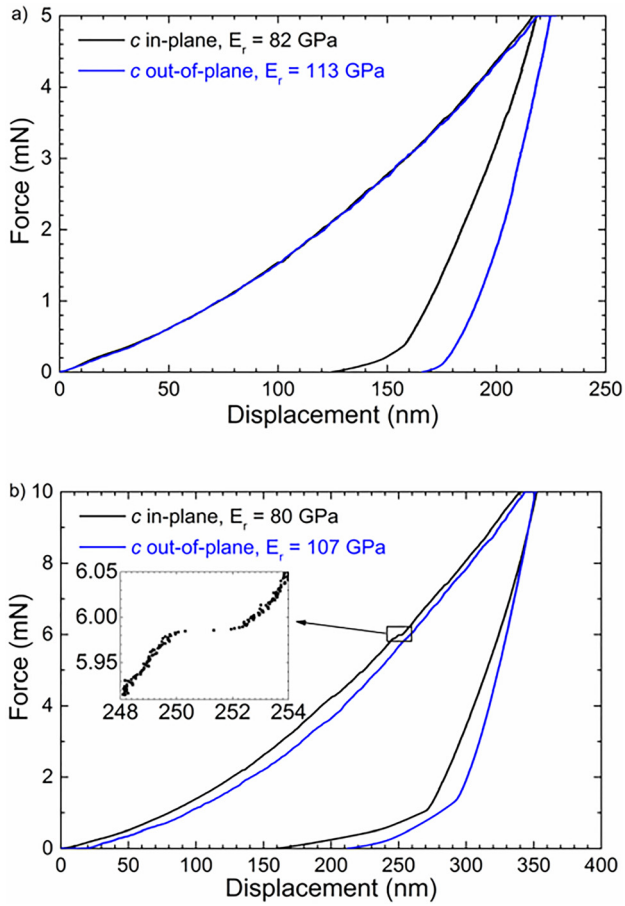

FIG. 1. Representative load-displacement curves of *c*-axis in-plane (black traces, *c*-axis perpendicular to the indentation axis) and out-of-plane (blue traces, *c*-axis parallel to the indentation axis) orientations subjected to maximum loads of (a) 5 mN and (b) 10 mN. The *c*-axis in-plane orientation displays pop-in during loading as indicated by the box and horizontal load-displacement (i.e., instantaneous displacement) region shown in the inset to panel (b), as well as greater elastic recovery during unloading compared to the *c*-axis out-of-plane. Conversely, the *c*-axis out-of-plane orientation exhibits a higher elastic modulus than the in-plane.

region shown in Fig. 1(b) inset] were observed for indentations on the *c*-axis in-plane orientation at both loads tested, similar to Aaltio *et al.*[22] Conversely, the load-displacement curves for the out-of-plane orientation did not demonstrate pop-ins, irrespective of load. The pop-ins observed in the *c*-axis in-plane indentation data were more pronounced at the higher 10 mN load than at the 5 mN load (see Figs. S3 and S4 in the supplementary material). Upon unloading, the rate of recovery below ~10% of the peak load (i.e., below ~0.5 mN for 5 mN peak loads and below ~1 mN for 10 mN peak loads) increased markedly. The increased recovery was larger for the in-plane than for the out-of-plane orientation.

TABLE I. Average (± one standard deviation) reduced elastic modulus measured at 5 mN and 10 mN peak loads for in-plane and out-of-plane *c*-axis orientations.

c-axis orientation	E_r (5 mN)	E_r (10 mN)
In-plane	84 ± 5 GPa	78 ± 1 GPa
Out-of-plane	122 ± 6 GPa	119 ± 11 GPa

B. Scanning probe microscopy

After indentation, the sample topography, indentation depth, and resultant magnetic response (in the form of magnetic stray fields) were measured using AFM/MFM.[15,16,18,23] To ascertain the effects of twinning on indentation recovery, the indented martensitic Ni-Mn-Ga sample was subsequently heated to above the austenite transition temperature (70 °C) and held at 81 °C for 10 min before being slowly cooled to room temperature and transformed back to the martensite phase.[23] The sample was then re-imaged with AFM/MFM. Indentation depths before and after the heating/cooling cycle were determined using a histogram to compare the bottom of an indent to the average height of the surrounding bulk material surface (similar to previous work,[18] no significant pile-up was observed, see Fig. S2 in the supplementary material for a representative high resolution AFM topography image of an indent). Recovery of the 10 mN load *c*-axis in-plane (top panel) and *c*-axis out-of-plane indents (bottom panel) after a heating/cooling cycle is depicted schematically and shown in the AFM topography images (brown color scale) in Fig. 2. The effect of the thermal cycle on the magnetic response due to the formation of self-accommodating martensite is also evident in the corresponding phase images in Fig. 2 (purple/pink/yellow color scale) and Figs. S5 and S6 in the supplementary material, as the changes in the number of twins and twinning orientation observed pre- and post-annealing [Figs. 2(b), 2(d), 2(g), and 2(i)] are associated with the development of self-accommodating martensite variants that form to minimize the strain energy of the indents upon cooling through the martensitic phase transition.

Opposite recovery behavior (negative rather than positive recovery) occurred for the two different *c*-axis orientations following thermal cycling through the martensite to austenite phase transition and back. For both loads tested (Table II), the *c*-axis in-plane indents showed positive recovery (i.e., a decrease in observed indentation depth following temperature/phase cycling), while the *c*-axis out-of-plane indents showed a negative recovery, i.e., an *increase* in depth.

Furthermore, samples that originally started out with their *c*-axis oriented out-of-plane (i.e., with the short, easy magnetization axis oriented parallel to the indentation axis) switched to a *c*-axis in-plane orientation following thermal cycling. The MFM phase contrast reveals the orientation of the *c*-axis, as the out-of-plane magnetization when the *c*-axis is perpendicular to the surface results in strong contrast (dark, vibrant colors in panel g of Fig. 2), whereas when the *c*-axis is parallel to the surface (panels b, d, and i of Fig. 2), the phase contrast is less (paler yellow and purple/pink). The sample with the *c*-axis initially oriented out-of-plane subjected to 5 mN indents showed a similar reorientation of the *c*-axis upon thermal cycling (Fig. 3). Additionally, at both loads, major twins formed along the diagonal of the nanoindentation array in conjunction with reorientation of the *c*-axis following thermal cycling.

IV. DISCUSSION

The decrease in reduced elastic modulus for the *c*-axis in-plane orientation relative to the out-of-plane orientation is

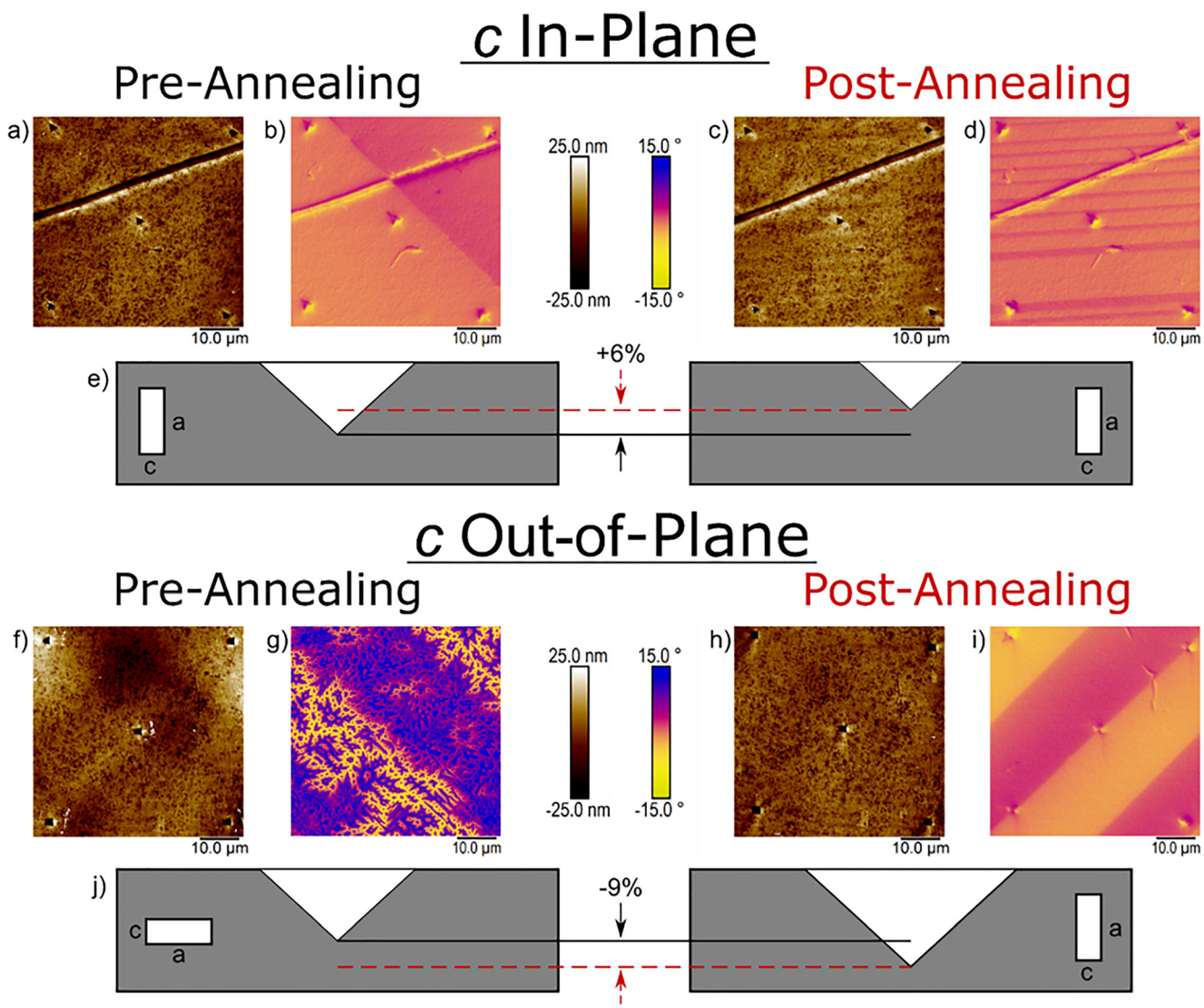

FIG. 2. AFM topography (a), (c), (f), and (h) and MFM magnetic response (b), (d), (g), and (i) of the *c*-axis in-plane [top panels, (a)–(e)] and out-of-plane [bottom panels, (f)–(j)] 10 mN indentations before (a), (b), (f), and (g) and after (c), (d), (h), and (i) thermal cycling through the martensite to austenite phase transition and back. The average recovery of the 10 mN *c*-axis in-plane indents was 6%, while the recovery of the 10 mN *c*-axis out-of-plane indents was negative (i.e., the indents increased in depth after thermal cycling through the phase transition), averaging −9%. Following thermal cycling, the *c*-axis orientation of the out-of-plane sample switched to in-plane (g) and (i), while the twins present in the in-plane sample increased in number and decreased in size (b) and (d) due to the formation of self-accommodating martensite.

likely related to elastic anisotropy for the differing *c*-axis orientations. Typically, the lattice stiffness, and hence the elastic modulus, increases with the decreasing lattice parameter, which agrees with the higher stiffness seen here on (001) compared to (100). Phonon dispersion curves measured with neutron scattering provide further insight into the elastic properties.[28] At small wave vector, the slopes of the [ξ00] and [00ξ] phonon branches are proportional to the corresponding sound wave velocities. Furthermore, the corresponding stiffness constants c_{11} and c_{33} are proportional to the square of the sound velocities. Neutron scattering shows that the sound velocity of longitudinal waves is slightly higher along [100] compared to [001], while the velocities of shear waves (contributing to the Poisson ratio) in these directions have the reverse order. For both cases, the differences are less than 20%, implying a variation in stiffness constants of about 40%. The stress state under an indentation tip is triaxial, and the reduced modulus results from a combination of the elements of the stiffness tensor. Thus, a direct comparison of the phonon spectra with the measured reduced moduli is not possible. However, the variation of normal and shear stiffnesses on the order of 40% deduced from the neutron scattering results[28] agrees with the variation in reduced moduli between the two *c*-axis orientations of about 50% reported here.

TABLE II. Average percent recovery (± one standard deviation) after thermal cycling for in-plane and out-of-plane *c*-axis orientations.

c-axis orientation	Recovery (5 mN)	Recovery (10 mN)
In-plane	14 ± 3%	6 ± 1%
Out-of-plane	−4 ± 2%	−9 ± 4%

Pop-ins typically stem from bursts of dislocations or stress-induced displacive phase transformations.[29] Ni-Mn-Ga is known to undergo stress-induced intermartensitic transformations,[30,31] which may cause the pop-ins. Pseudoelastic

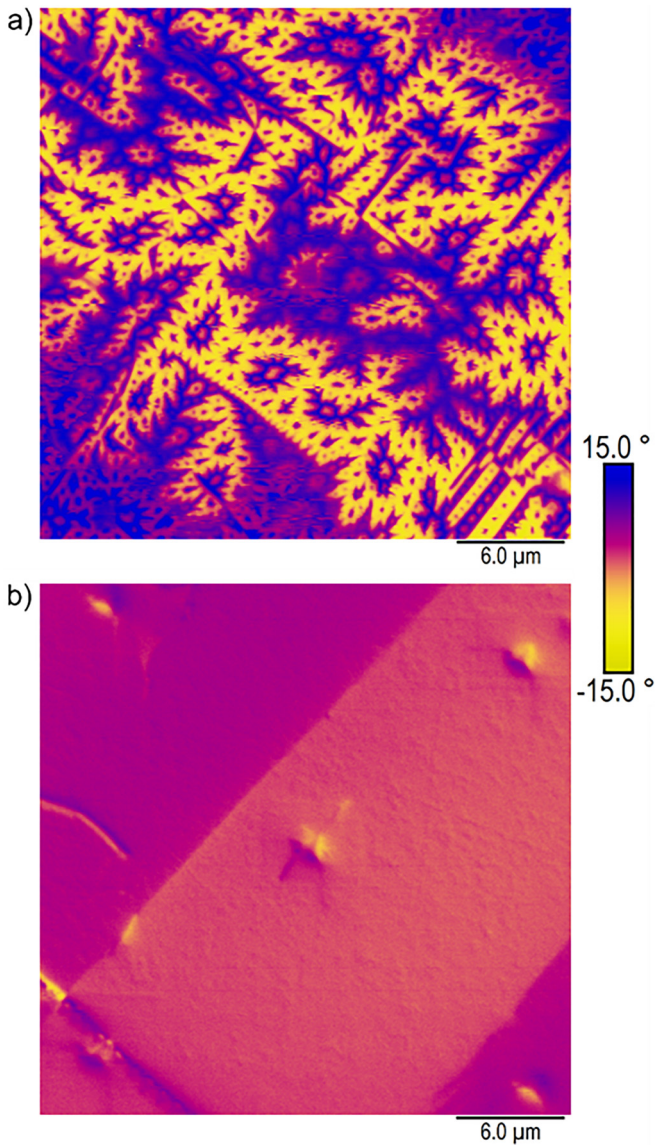

FIG. 3. Magnetic response of a *c*-axis out-of-plane sample subjected to a centered square array of 5 mN indents (a) before and (b) after a heating and cooling cycle through the martensitic-austenitic transformation. After thermal cycling, the *c*-axis orientation has switched to in-plane, as evidenced by the significant decrease in MFM phase contrast.

twinning is another potential cause for this effect. In either case (i.e., intermartensitic transformation or pseudoelastic twinning), unloading reverses the deformation, albeit on a different (slower) timescale. While the pop-ins are instantaneous, which is typical for both stress-induced phase transformations and pseudoelastic twinning, the reverse effect may exhibit hysteresis and be slower to form. Both effects can stem from the interaction of the phase boundary/twin boundary with point and other defects. These relaxation effects may cause the significant elastic recovery that occurs during unloading for the *c*-axis in-plane orientation. In contrast, the *c*-axis out-of-plane orientation does not demonstrate pop-in behavior, while also exhibiting a much smaller elastic recovery, as seen in the load-displacement curves (Figs. 1 and S3 and S4).

Because both the *c*-axis in-plane and out-of-plane Ni-Mn-Ga surfaces studied here were electropolished, the dislocation density within each should be consistent.[22] Thus, the lack of pop-in for the *c*-axis out-of-plane orientation suggests that a mechanism other than dislocations must be responsible for the observed difference in load-displacement behavior. In particular, the difference in elastic recovery during unloading for the two orientations may be attributable to pseudoelasticity caused by displacive transformations[32,33] or twinning. Pseudoelastic twinning is enabled when surface stress concentrations, such as those induced by nanoindentation, are present. The de-twinning phenomenon occurs when the image force of the twin is larger than the force experienced through internal stresses, resulting in partial recovery of plastic deformation following unloading for the *c*-axis in-plane samples.[15] As Ni-Mn-Ga twins deform during loading, apparent stiffness may decrease. This phenomenon can be attributed to elastic anisotropy, indicating that dislocation activity depends not only on dislocation density but also on crystallographic orientation.[34] If the pop-ins are caused by an intermartensitic transformation, the transformation enthalpy provides the driving force for recovery.

In either case, i.e., twinning or intermartensitic transformation, the driving force for the deformation process is the work done by the moving interface. This work is the product of stress, twinning or transformation strain, and volume. In both cases, the strain depends on the initial orientation of the lattice. While details depend on the entire strain tensor (and on the inhomogeneous stress state), the deformation perpendicular to the surface plays a dominant role. In particular, if the short *c*-axis is perpendicular to the surface (i.e., for the out-of-plane orientation), the transformation strain is smaller than when the long *a*-axis is perpendicular to the surface (i.e., for the in-plane orientation). This is true for both twinning and intermartensitic transformations. Therefore, regardless of the mechanism (i.e., pseudoelastic twinning or intermartensitic transformation), the driving force for pop-ins is smaller for the *c*-axis out-of-plane orientation compared to the in-plane orientation, leading to a higher likelihood of observing pop-ins for the in-plane orientation.

Similar to Ni-Mn-Ga, the combination of instrumented nanoindentation with a Berkovich diamond tip indenter followed by AFM imaging of the resultant indents has been used previously in studies on the NiTi shape memory alloy nitinol to examine indentation recovery on the nanoscale following thermal cycling through the martensite to austenite phase transition.[24–26] In contrast to these studies on nitinol however, which found significant (>30%) recovery following thermal cycling, we found limited recovery of the plastic deformation for Ni-Mn-Ga. In fact, the *c*-axis out-of-plane orientation exhibited a *negative* recovery (Fig. 2), meaning that the indentation depth increased after thermal cycling through the martensitic-austenitic phase transition. Conversely, for the initial *c*-axis in-plane samples, a positive recovery of the indents upon thermal cycling was seen, albeit to a lesser degree than for nitinol.[24–26] However, rather than a 90° shift in the *c*-axis, an increased number of self-accommodating in-plane martensite variants formed to minimize the strain energy of the indents upon cooling through the martensitic phase transition, perhaps via pseudoelastic twinning. Although in-plane variants should cancel if the sample was perfectly cut along

{100}, resulting in no net effect on the indent depth, slight misalignments of the variants relative to the surface plane are evident based on the contrast present in the corresponding MFM phase images [Figs. 2(d), S5b, and S6b]. Thus, the multivariant nature of the sample following thermal cycling may be the cause of some of the variability in the magnitude of recovery seen in Table II due to imperfect canceling leading to a slight net change in *c*-axis alignment relative to the surface.

Additionally, because Ni-Mn-Ga is magnetic, MFM enabled determination of *c*-axis orientation and direct visualization of twinning at the nanoscale, which is not possible in the case of NiTi shape memory alloys. A higher resolution MFM image of one of the indents (Fig. 4) shows that the indentation did not affect the magnetic structure. Twinning events change the magnetic structure through a reorientation of the *c*-axis. The absence of contrast variations in the MFM images indicates that twinning does not contribute to the plastic deformation in the indent.

The slope angle of the Berkovich tip is 24.65°, and the measured slope of the indents is very close to this value. This is about six times larger than the surface deformation caused by twinning in 10M martensite.[23] The strains accommodated by intermartensitic transformations and other stress-induced transformations are of the same order of magnitude as the twinning shear. Therefore, twinning and stress-induced phase transformations are not sufficient to accommodate the permanent indentation deformation. We conclude that most likely indentation occurs via dislocation plasticity.

This is a surprising result since Ni-Mn-Ga is brittle, at least in polycrystalline form where the twin-grain boundary interaction causes intercrystalline fracture.[35,36] The reason lies in substantial tensile stresses arising when a twin is blocked at a grain boundary[37,38] and the lack of sufficient shear systems ensuring deformation compatibility across the grain boundary. Both arguments are not relevant here however because of the absence of grain boundaries and a large compressive hydrostatic stress component.[39]

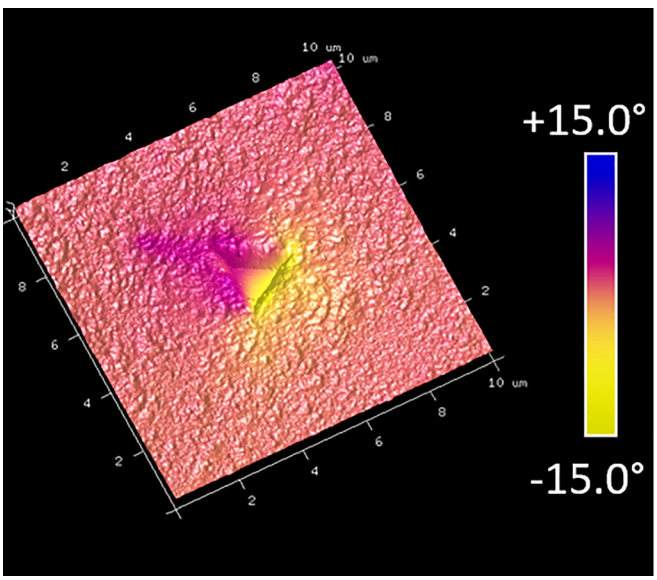

FIG. 4. High resolution image of the central indent in a centered square array of 10 mN indents on a *c*-axis in-plane sample prior to heating through the martensitic-austenitic transformation. Magnetic phase (color scale) overlaid on 3D rendering of topography showing that the indentation did not affect the magnetic structure.

The indentations did not form hillocks. This indicates that the deformation field reaches far into the bulk of the material. Otherwise, a high degree of densification would be required to accommodate the compressive deformation locally, which is unlikely. A far reaching deformation field may impact the martensitic transformation during the heating/cooling experiments that followed the indentation experiments. In particular, a large deformation field with a compressive strain component perpendicular to the surface has a large intrinsic stress component in that direction. This stress component may favor the formation of in-plane oriented martensitic domains to minimize strain energy and thus, the switching from out-of-plane to in-plane orientation [Figs. 3, 2(g), and 2(i)] as a result of the heating-cooling cycle. This change in *c*-axis orientation is likely the cause of the increase in the indentation depth, as the switching of the crystallographic orientation is accompanied by a 6% strain, which is on the order of the observed negative recovery. This is similar to what one would expect to see upon application of an appropriately aligned magnetic field or mechanical force to cause reorientation of the easy magnetization or *c*-axis. Although the change in orientation following thermal cycling may be coincidental, it was found to be reproducible, occurring for all *c*-axis out-of-plane indents subjected to thermal cycling (both 5 mN and 10 mN loads; see Figs. 2 and 3, also Figs. S5 and S6 in the supplementary material), including across multiple samples (a replicate sample prepared from a different crystal of the same composition was studied at a single nanoindentation load of 10 mN and exhibited the same behavior as shown here).

The change in orientation could be triggered by residual stresses around the indentation which may bias the martensitic transformation. Such an effect is used to bias the martensitic transformation in thermal shape memory alloys to create a two-way shape memory effect.[40,41] Furthermore, in contrast to previous studies on Ni-Mn-Ga where the sample was constrained during thermal cycling either by application of an external magnetic field[42] or a constant mechanical load,[23] in the current study, the sample was unconstrained. It is unlikely that extrinsic forces triggered the switching of the *c*-axis orientation.

V. CONCLUSIONS

The nanomechanical properties and behavior of electropolished single crystalline 10M martensitic $Ni_{51}Mn_{27}Ga_{22}$ samples with the crystallographic *c*-axis oriented in-plane versus out-of-plane were determined via nanoindentation. The results show a significant difference in load-displacement behavior and elastic modulus for *c*-axis in-plane versus out-of-plane, with the out-of-plane modulus being about 50% higher. Differences in elastic modulus are attributed to elastic anisotropy. Pop-in and greater elastic recovery upon unloading occurred for the crystallographic *c*-axis in-plane orientation, perhaps due to pseudoelastic twinning or intermartensitic transformations, while indents on surfaces with the *c*-axis out-of-plane experienced limited elastic recovery. The complementary non-destructive

techniques of AFM and MFM were then applied to probe the twinning structure of the indented samples. The absence of contrast variations in the MFM images indicated that twinning does not contribute to the plastic deformation in the indent, which is instead likely due to dislocation plasticity. However, differences in the twin structure (orientation, number, etc.) were observed upon thermal treatment of the indented samples: following heating of the samples to above the martensite to austenite phase transition temperature and subsequent cooling back to the martensite form at room temperature, samples initially oriented with their *c*-axis out-of-plane converted to a *c*-axis in-plane orientation. In contrast, *c*-axis in-plane samples responded to thermal cycling with an increase in the number of twins and a concomitant decrease in the twin size. The driving force behind both processes is likely minimization of the strain energy of the indents. Given the significant differences in nanomechanical properties and behavior reported here for the *c*-axis in-plane and out-of-plane orientations, further studies evaluating nanoscale phenomena may provide additional insights into the mechanisms of twin boundary motion and surface stress relief. With enhanced understanding and control of the nanoscale structure and *c*-axis alignment of Ni-Mn-Ga, its orientation-dependent nanomechanical behavior can then be harnessed for use in MSMA devices.

SUPPLEMENTARY MATERIAL

See supplementary material for further details regarding experimental methods, including Ni-Mn-Ga sample preparation (polishing and magnetic alignment procedures), nanoindentation (array creation and martensite-austenite phase transition), scanning probe microscopy (AFM and MFM), and data analysis (Young's modulus and indentation depth determination). Additional figures and tables presenting all nanoindentation, AFM, and MFM results are also included in the supplementary material.

ACKNOWLEDGMENTS

We thank Dr. Tony Hobza for helpful discussions and insights into the effect of the internal magnetic field on the magnetomechanics of Ni-Mn-Ga. Financial support from the National Science Foundation, Project No. NSF-CMMI-1068069, is gratefully acknowledged.

[1]K. Ullakko, J. Huang, C. Kantner, R. O'Handley, and V. Kokorin, Appl. Phys. Lett. **69**, 1966 (1996).
[2]A. Sozinov, N. Lanska, A. Soroka, and W. Zou, Appl. Phys. Lett. **102**, 021902 (2013).
[3]J. Tellinen, I. Suorsa, A. Jääskeläinen, I. Aaltio, and K. Ullakko, in *Basic Properties of Magnetic Shape Memory Actuators in Proceedings of the 8th International Conference on New Actuators, Bremen, Germany, June 10-12, 2002*, edited by H. Borgmann (Messe Bremen, Bremen, Germany, 2002), p. 566.
[4]M. A. Marioni, R. C. O'Handley, and S. M. Allen, Appl. Phys. Lett. **83**, 3966 (2003).
[5]O. Y. Kanner, D. Shilo, J. Sheng, R. D. James, and Y. Ganor, Smart Mater. Struct. **22**, 085030 (2013).
[6]A. R. Smith, J. Tellinen, and K. Ullakko, Acta Mater. **80**, 373 (2014).
[7]N. J. Kucza, C. L. Patrick, D. C. Dunand, and P. Müllner, Acta Mater. **95**, 284 (2015).
[8]S. Barker, E. Rhoads, P. Lindquist, M. Vreugdenhil, and P. Müllner, J. Med. Devices **10**, 041009 (2016).
[9]L. Straka, N. Lanska, K. Ullakko, and A. Sozinov, Appl. Phys. Lett. **96**, 131903 (2010).
[10]R. Tickle and R. James, J. Magn. Magn. Mater. **195**, 627 (1999).
[11]O. Heczko, A. Sozinov, and K. Ullakko, IEEE Trans. Magn. **36**, 3266 (2000).
[12]H. Karaca, I. Karaman, B. Basaran, Y. I. Chumlyakov, and H. Maier, Acta Mater. **54**, 233 (2006).
[13]Y. Ganor, D. Shilo, T. W. Shield, and R. D. James, Appl. Phys. Lett. **93**, 122509 (2008).
[14]D. C. Dunand and P. Müllner, Adv. Mater. **23**, 216 (2011).
[15]P. Müllner, Z. Clark, L. Kenoyer, W. B. Knowlton, and G. Kostorz, Mater. Sci. Eng., A **481–482**, 66 (2008).
[16]M. Reinhold, D. Kiener, W. B. Knowlton, G. Dehm, and P. Müllner, J. Appl. Phys. **106**, 053906 (2009).
[17]A. Jakob, M. Müller, B. Rauschenbach, and S. Mayr, New J. Phys. **14**, 033029 (2012).
[18]C. S. Watson, C. Hollar, K. Anderson, W. B. Knowlton, and P. Müllner, Adv. Funct. Mater. **23**, 3995 (2013).
[19]R. Niemann, S. Hahn, A. Diestel, A. Backen, L. Schultz, K. Nielsch, M.-X. Wagner, and S. Fähler, APL Mater. **4**, 064101 (2016).
[20]L. Zhou, A. Giri, K. Cho, and Y. Sohn, Acta Mater. **118**, 54 (2016).
[21]Y. Ganor and D. Shilo, Appl. Phys. Lett. **93**, 031905 (2008).
[22]I. Aaltio, X. Liu, M. Valden, K. Lahtonen, O. Söderberg, Y. Ge, and S. Hannula, J. Alloys Compd. **577**, S367 (2013).
[23]M. Reinhold, C. Watson, W. B. Knowlton, and P. Müllner, J. Appl. Phys. **107**, 113501 (2010).
[24]G. A. Shaw, D. S. Stone, A. D. Johnson, A. B. Ellis, and W. C. Crone, Appl. Phys. Lett. **83**, 257 (2003).
[25]G. A. Shaw, J. S. Trethewey, A. D. Johnson, W. J. Drugan, and W. C. Crone, Adv. Mater. **17**, 1123 (2005).
[26]C. P. Frick, T. W. Lang, K. Spark, and K. Gall, Acta Mater. **54**, 2223 (2006).
[27]W. C. Oliver and G. M. Pharr, J. Mater. Res. **7**, 1564 (1992).
[28]S. Ener, T. Mehaddene, B. Pedersen, M. Leitner, J. Neuhaus, and W. Petry, New J. Phys. **15**, 123016 (2013).
[29]C. A. Schuh, Mater. Today **9**, 32 (2006).
[30]V. Chernenko, J. Pons, E. Cesari, and K. Ishikawa, Acta Mater. **53**, 5071 (2005).
[31]V. Chernenko, E. Villa, D. Salazar, and J. Barandiaran, Appl. Phys. Lett. **108**, 071903 (2016).
[32]K. Otsuka, H. Sakamoto, and K. Shimizu, Acta Metall. **27**, 585 (1979).
[33]J. E. Bradby, J. S. Williams, and M. V. Swain, Phys. Rev. B **67**, 085205 (2003).
[34]J. J. Vlassak and W. Nix, J. Mech. Phys. Solids **42**, 1223 (1994).
[35]U. Gaitzsch, M.Sc. thesis, Technische Universität Dresden, 2008.
[36]A. Gilbert, G. T. Hahn, C. N. Reid, and B. A. Wilcox, Acta Metall. **12**, 754 (1964).
[37]M. H. Yoo, Metall. Trans. A **12**, 409 (1981).
[38]P. Müllner, C. Solenthaler, P. J. Uggowitzer, and M. O. Speidel, Acta Metall. Mater. **42**, 2211 (1994).
[39]S. Suresh and A. E. Giannakopoulos, Acta Mater. **46**, 5755 (1998).
[40]M. Frensemeier, E. Arzt, E. Qin, C. P. Frick, and A. S. Schneider, MRS Commun. **5**, 77 (2015).
[41]S. A. Brinckmann, M. Frensemeier, C. M. Laursen, H. J. Maier, D. Britz, A. S. Schneider, F. Mücklich, and C. P. Frick, Mater. Sci. Eng., A **675**, 253 (2016).
[42]Q. Pan and R. D. James, J. Appl. Phys. **87**, 4702 (2000).